Role of effective tensile strain in electromechanical response of helical graphene nanoribbons with open and closed armchair edges

D.-B. Zhang and T. Dumitrică

Phys. Rev. B **85**, 035445 — Published 27 January 2012

DOI: 10.1103/PhysRevB.85.035445

Role of the effective tensile strain in the electromechanical response of helical graphene nanoribbons with open and closed armchair edges

D.-B. Zhang[1] and T. Dumitrică[1,2,*]
[1]*Department of Mechanical Engineering,* [2]*Department of Chemical Engineering and Materials Science, University of Minnesota, Minneapolis, MN 55455, USA*
(Dated: December 29, 2011)

There is a growing need to understand the and mechanical and electronic properties of non-ideal graphene nanoribbons. Using objective molecular dynamics and a density-functional based tight-binding model, we investigate the effects of torsion on the electromechanical properties of graphene nanoribbons with armchair edges. We propose to characterize with an effective tensile strain scalar the torsional mechanical response, including a reverse Poynting effect, and the fundamental band gap modulations. The demonstrated utility of this concept in both the mechanical and electrical domains provides a perspective for understanding electromechanical response in a unified way, and for designing NEMS devices with graphene components.

PACS numbers: 73.22.Pr, 62.25.-g, 61.48.Gh

I. INTRODUCTION

Opening a band gap in graphene is an important current research topic. Graphene nanoribbons (GNRs), new one-dimensional materials derived from graphene, present special importance because the lateral quantum confinement provides one route for band gap opening and manipulation. Unfortunately current GNRs fabrication methodologies don't yet allow for a precise control of GNRs width and edges, and thus for precise band gap design. However, we note two promising developments[2,3]: In one approach[3], narrow helically-twisted GNRs with open edges were formed within a single-walled carbon nanotube (CNT). The role of the CNT was to confine growth in one dimension and determine the GNR's width. In another technique[2], edge-closed GNRs with enhanced conductivity were achieved after removal of the metal nanowire on which they were grown.

Twisting, a primary deformation mode for macroscopic slender elements, can be imposed with relative ease on nano-scale elements, including single- and multi-walled CNTs[4–7]. Experiments found that the electronic structure of CNTs are very sensitive to the torsional deformation. In terms of theoretical modeling, the idealized model of Yang and Han[8] (YH) formulated in terms of simple π-orbitals tight-binding treatment, is widely used to rationalize the intrawall band-gap variations with twist. The model gives the fundamental band gap variation in cylindrical CNTs under a homogeneous strain. Moreover, it reveals that the electronic response of CNT is selective to different pure deformation modes. For example, in any zigzag CNT, the valence and conduction bands are coupled to an applied tensile strain but decoupled from any shear strain stored in the CNT wall.

Although of practical importance, the electromechanical behavior of twisted GNRs is less understood. Microscopic modeling of twisted nanoribbons is not straightforward. The use of periodic boundary conditions (PBC) is inconvenient as it requires large translational supercells and can describe only discrete torsional deformations compatible with the assumed translational symmetry. Twisted GNRs have been studied in Möbius-like topologies[9], which also allows little control over the imposed twist rate.

In this article we model the electromechanical properties of uniformly twisted GNRs with H-terminated and closed armchair edges with objective molecular dynamics (MD)[10,11] and a density-functional-based tight binding (DFTB) model[12] extended to capture the long range van der Waals interactions[13]. Remarkably, the method allows for simulating GNRs under an arbitrary twist value and study the coupling of twisting with axial deformation. We show that twisting without allowing for axial relaxation provides an effective way to manipulate the band gap of these two GNR types. Their electromechanical response can be understood in an unified way by using the notion of effective strain.

II. COMPUTATIONAL METHOD

The DFTB objective MD method was implemented by us in the code Trocadero[14] and used early on in Ref.[15] to simulate the electromechanical response of single- and multi-walled armchair CNTs in torsion. In DFTB, only the the valence shell consists of four *sp* orbitals are considered to describe the electronic states. In objective MD, we describe an infinitely long twisted structure from the N_0 atoms belonging to the the primitive translational cell of the corresponding untwisted structure. Let $\mathbf{X}_j$ be their atomic positions of these N_0 atoms. Using the concept of objective structures[16], the $\mathbf{X}_{j,\zeta}$ atomic positions in the primitive cell replica indexed with an integer $\zeta = 0, ..., \infty$ are given by

$$\mathbf{X}_{j,\zeta} = \mathbf{R}^{\zeta}\mathbf{X}_j + \zeta\mathbf{T}, \quad j = 1, ..., N_0. \tag{1}$$

Rotational matrix **R** of angle θ combined with axial vector **T** characterizes the helical repeating rule replacing the standard translation. The above equation replaces the usual PBC boundaries. A pure twist rate γ is imposed by setting $\theta = \gamma|\mathbf{T}|$. The symmetry-adaptation of the electronic wavefunction to eq. (1) is described in Ref.[11].

We illustrate the importance of direct objective MD simulations over the YH predictions with a brief initial study of twisted zigzag cylindrical CNTs. It is long known that elastic rods or tubes made out of simple solids elongate when subjected to torsion[17]. To investigate whether this Poynting effect is present in CNTs, our calculations were conducted by performing conjugate gradient relaxations at fixed θ first under the $|\mathbf{T}|$ corresponding to the stress-free untwisted structure and next under relaxed $|\mathbf{T}|$. An axial Poynting strain ε^{Py} is calculated from the difference in $|\mathbf{T}|$ values.

Indeed, we regain the expected behavior, as the relaxed structure elongates. Fig. 1(a) displays the results of a systematic investigation on a collection of zigzag CNTs with different R. We obtained that ε^{Py} follows the expected[17] linear dependence on γ^2, Fig. 1(a) left. The spread over R in Fig. 1(a) left is eliminated when the same data is plotted against γ^2R^2 in Fig. 1(a) right. Here γR represents the shear strain experienced by the cylindrical CNT wall. More precisely, the atomistic data gives $\varepsilon^{Py} = 0.54\gamma^2R^2$. Concerning the response of the electronic states, our calculations indicated that the YH predictions should be taken with caution at large shear deformations. For example, the band gap variations of a twisted (48,0) CNT, Fig. 1(b), demonstrate that there is a significant band gap opening at a large twist rate ($\gamma > 1$ deg/nm). What is also interesting is that the two curves corresponding to fixed and relaxed $|\mathbf{T}|$ become distinct at large γ. Thus, the axial strain created in response to the imposed large shear contributes to the band gap modulations as well (although to a smaller extent in comparison with the shear deformation).

III. MECHANICAL RESPONSE

For the structures of interest here, uniformly twisted GNRs with H-terminated, Fig. 2(a), and closed armchair edges, Fig. 3(a), the twist-induced axial strain is of prime importance, as it dominates their gapping. Before discussing our results, let us actualize our earlier predictions[10,18,19] that these structures are prone to an inverse Poynting effect: when twisted they tend to shrink. Interestingly, the compressive ε^{Py} still depends linearly on γ^2, Fig. 2(b) and Fig. 3(b). To understand the origin of this behavior, it is important to summarize our previous results[18,19]: Firstly, under the same γ, GNRs are much less sheared than cylindrical CNTs. In particular, twisted GNRs with open edges have no shear. Consequently, a direct Poynting effect caused by the shear deformation would be very small. Secondly, the distribution of tensional strain stored in twisted GNRs is inhomogeneous, with the outermost dimer lines being the most stretched, a behavior that can be also seen in Figs. 2(a) and 3(a). Finally, the band gap response of twisted GNRs with armchair open edges is determined by an effective tensile strain, defined as $\varepsilon^{eff} = \frac{1}{N}\sum_{n=1}^{N}\varepsilon_n$. Here ε_n is the local tensile strain along the dimer line n.

The inverse Poynting effect observed in our simulations is triggered by an axial tensile stress σ associated to the twist-induced inhomogeneous tensile strain. To express σ, we employ a continuum membrane description of the one-atom thick layer with two parameters, the in-plane stiffness $C = 59$ eV/atom and Poisson ratio $\nu = 0.26$. The local tensile stress under the local tensile strain ε_n is obtained with Hooke's law as $C/(1-\nu^2)\varepsilon_n$. We then approximate σ as an average of the local tensile stress,

$$\sigma \approx \frac{1}{N}\sum_{n=1}^{N}\sigma_n = \frac{1}{N}\sum_{n=1}^{N}\frac{C}{1-\nu^2}\varepsilon_n = \frac{C}{1-\nu^2}\varepsilon^{eff}. \tag{2}$$

Here, the small effect from the difference in elastic stiffness between the edge and inner part of GNRs is omitted. Once $|\mathbf{T}|$ is allowed to relax, the twisted GNR shrinks until σ eventually vanishes. Thus, the axial strain $-\varepsilon^{Py}$ associated to the Poynting effect should be close to ε^{eff}, in agreement with the atomistic data shown in Fig. 2(b) and Fig. 3(c).

We further detail the utility of the scalar ε^{eff} (and not γ) to characterize the mechanical response of twisted GNRs with open edges. On one hand, one is is tempted to study the stress-strain relation of these structures with the derivative of the total energy E_{tot} to twist rate γ. However, in Fig. 4(a) we obtained an unusual nonlinear behavior of $dE_{tot}/d\gamma$. On the other hand, in Fig. 4(b) the derivative of the total energy E_{tot} to ε^{eff} becomes linear in ε^{eff} with a slope of 61.3 eV, in good agreement with the predicted $C/(1-\nu^2)$ parameter. Focussing on the tensile strain energy component of the total GNR energy, for an armchair GNR with N dimer lines, this writes

$$E_s \approx \frac{1}{N}\sum_{n=1}^{N}\frac{1}{2}\frac{C}{1-\nu^2}\varepsilon_n^2 = \frac{\gamma^4}{8N}\sum_{n=1}^{N}\frac{C}{1-\nu^2}d_n^4. \tag{3}$$

Here d_n is the distance of the dimer line with index n to the GNR axis and $\varepsilon_n = \frac{1}{2}\gamma^2 d_n^2$ was used. Thus, $dE_s/d\gamma \sim \gamma^3$.

If instead we introduce the effective strain with $\varepsilon_n = \varepsilon^{eff} + \varepsilon_n^0$ and using the evident relation $\sum_{n=1}^{N}\varepsilon_n^0 = 0$, we have

$$E_s \approx \frac{1}{2}\frac{C}{1-\nu^2}\left(\varepsilon^{eff}\right)^2 + \frac{1}{N}\sum_{n=1}^{N}\frac{1}{2}\frac{C}{1-\nu^2}\left(\varepsilon_n^0\right)^2. \tag{4}$$

We label the first term with E_{eff} and second term with $O(E)$. Thus, confirming eq. (2), $\sigma \approx dE_s/d\varepsilon^{eff} \approx \varepsilon^{eff} C/(1-\nu^2)$. When $|\mathbf{T}|$ is kept fixed, E_{eff} is the dominant component of the strain energy. If $|\mathbf{T}|$ is allowed to relax at each imposed θ, ε^{eff} vanishes for the linear elastic case. However, in practice there is still a small residual ε^{eff} due to the intrinsic elastic nonlinearity in the chemical bonds[18].

In Fig. 4(b), the unusual upwards shift from the line $\varepsilon^{eff} C/(1-\nu^2)$ by ~ 0.35 eV is due to the misalignment of π orbitals to the total energy. Indeed, unlike the flat case, the π-orbitals are no longer parallel with each other but rotated according to the their axial location. We evaluated the energy contribution due to the π-orbital misalignment E_π by computing the adjustment in hopping integrals between rotated π-orbitals located on the nearest carbon atoms. Note that unlike in graphene under pure bending case[20], the two faces of the twisted GNR are equivalent. Thus, there is no π charge spill from one site to the other, i.e., no shift in the sp^2 hybridization at any atomic site. Consider the two atoms (see the insert) highlighted in Fig. 2(a). The misalignment angle between the two π-orbitals located on these two atoms due to a twist rate γ is simply γa_{C-C}, where $a_{C-C} = 1.42$ Å is the carbon-carbon bond length. Let $t_0 = 2.8$ eV be the nearest neighborhood hopping parameter for aligned π-orbitals. The strain energy associated with the twist induced misalignment is $\sim 2\sqrt{3}\gamma^2 a_{C-C}^2 t_0/3$. The $\sqrt{3}$ factor reflects the resonance bonding correction[20]. For the whole GNR with N dimer lines we obtain

$$E_\pi \approx 0.04 t_0 |\mathbf{T}|^2 \gamma^2 = D\varepsilon^{eff}. \tag{5}$$

Here, $D = 1.28 t_0 |\mathbf{T}|^2/(N^2-1)a_{C-C}^2$ and

$$\varepsilon^{eff} = \gamma^2 \frac{1}{2N}\sum_{n=1}^{N} d_n^2 = \gamma^2 \frac{1}{32}(N^2-1)a_{C-C}^2. \tag{6}$$

For the 12 GNR, the above model gives $D = 0.23$ eV, in good agreement with the intersect of $dE_{tot}/d\varepsilon^{eff}$ in Fig. 4(b).

In summary, the above insights suggest the following decomposition of the DFTB computed energy

$$E_{tot} \approx E_{eff} + E_\pi + O(E) = \frac{1}{2}\frac{C}{1-\nu^2}\left(\varepsilon^{eff}\right)^2 + D\varepsilon^{eff} + O(E). \tag{7}$$

Although E_{eff} is the dominant component, E_π, a quantum mechanical quantity which cannot be captured by the continuum membrane model[20], is still visible in Fig. 4(c). Note that for open edges saturated with other chemistry, the above equation should be further enhanced to include edge energies[21].

IV. ELECTRONIC RESPONSE

Twisted armchair GNRs with open and closed edges exhibit fundamental band gap modulations, Fig. 5. The utility of ε^{eff} to describe gapping of GNRs with open edges[18] is confirmed in Fig. 5(a) for the twisted 12 GNR. The quadratic band gap variation with γ, Fig. 5(a) left, turn into linear variations with ε^{eff}, Fig. 5(a) right, as expected for a GNR under uniaxial tension[22,23]. We recall[18] that the linear band gap–ε^{eff} has a slope of $\sim 3t_0(1+\nu)$ and an oscillation period of $2\pi/[3(1+\nu)(N+1)]$. According to YH model, these are also the characteristics for a $(N+1,0)$ CNT in tension.

A $2N$ GNR with two closed armchair edges[3] is essentially a collapsed[24,25] $(N,0)$ CNT. The two opposite walls with one-atom thickness facing each other with a separation of 3.4 Å are mediated by van der Waals forces. While the two walls stack mostly with a A-B pattern in collapsed armchair CNTs[19], here we obtain an intermediate stacking pattern between A-A and A-B in zigzag CNTs, Fig. 2(a). Therefore, the bilayer coupling should play little role in gapping[19,24]. We focus our attention on the intra-wall strain and show that gapping of these structures is determined by ε^{eff}, Fig. 5(b). To characterize the coupling of the conduction and valence bands to twisting, we actualize the effective strain theory[19] where the influence of inhomogeneous local tensile strain on electronic energetic state is derived with a perturbative π-orbital orthogonal tight-binding.

In the "helical-angular" representation, a cylindrical $(N,0)$ CNT is described with a two-atom objective cell as

$$\mathbf{X}_{j,(\zeta_1,\zeta_2)} = \mathbf{R}_2^{\zeta_2}\mathbf{R}_1^{\zeta_1}\mathbf{X}_j^0 + \zeta_1\mathbf{T}_1,\ j = 1,2. \tag{8}$$

Index j runs over the A and B atoms at locations $\mathbf{X}_j^0$ inside the repeating objective domain. Integers $\zeta_1 = 0,...,N_s$ (where N_s is typically ∞) and $\zeta_2 = 0,...,N-1$ label various replicas of this domain. Rotational matrix $\mathbf{R}_1$ of angle $\theta_1 = \pi/N$ and the axial vector $\mathbf{T}_1$ of length $\sim \frac{3}{2}a_{C-C}$ indicate a helical transformation applied to the objective domain. Rotational matrix $\mathbf{R}_2$ indicates the angular operation, an axial rotation of angle $\theta_2 = 2\pi/N$.

In this representation, the π electronic eigenstates of energies $E_{n\kappa}$ are labeled by a helical quantum number $-\pi \le \kappa < \pi$ and $n = 0,1,...,N-1$. They are obtained in terms of two symmetry-adapted Bloch sums:

$$|j,n\kappa\rangle = \frac{1}{\sqrt{N_s N}}\sum_{\zeta_n=0}^{N_s-1}\sum_{\zeta_2=0}^{N-1} e^{i\kappa\zeta_1 + in\theta_2\zeta_2}|j,\zeta_1\zeta_2\rangle. \tag{9}$$

Here $|j,\zeta_1\zeta_2\rangle$ is the atomic π-orbital located on the atom j in the objective domain indexed by ζ_1 and ζ_2. If follows that the π electronic energy dispersion writes[19]

$$E_{n\kappa}^2 = \left| \sum_{\eta} t_\eta(\varepsilon) f_\eta(n,\kappa) \right|^2 . \tag{10}$$

Here integer $\eta = 1,2,3$ indicates the sum running over the three nearest neighboring atoms of a carbon atom and t_η is the corresponding π-orbital hopping parameters while f_η is the relative Bloch phase for the neighbor atom indexed with ζ.

Under homogeneous tensile strain ε (in the YH model) the effect of ε is included in eq. (10) via the variation of the hopping parameter with ε. To first order in ε, the resulted variations of the hopping parameters in the axial and lateral directions are $2t_0\varepsilon$ and $0.5t_0(1-3\nu)\varepsilon$, respectively[18]. Under inhomogeneous tensile strain, the hopping parameter t_η varies according to the local tensile strain ε_n at each "helical angular" objective cell. The π electronic energy dispersion now becomes

$$E_{n\kappa}^2 \approx \left| \frac{1}{N} \sum_{n,\eta} t_\eta(\varepsilon_n) f_\eta(n,\kappa) \right|^2 \approx \left| \sum_{\eta} t_\eta(\varepsilon^{eff}) f_\eta(n,\kappa) \right|^2 . \tag{11}$$

Note that in the above, $(1/N)\sum_n t_\eta(\varepsilon_n) \approx t_\eta(\varepsilon^{eff})$ stands under the expansion of t_η to the first order in ε_n. What is important is that the last expression in eq. (11) indicates that the band gap variations should still follow the ideal YH behavior but under ε^{eff}.

The above predictions of the band gap variations with twist agrees well with the direct objective MD calculations: When plotted against ε^{eff} extracted from the DFTB data, the band gap variations for the 96 GNR display the YH behavior of a cylindrical (48,0) CNT under tension, Fig. 5(b). Thus, the variety of other factors, like the effective shear strain[19] stored in the wall, the bilayer coupling across opposite faces, the misalignment of the π orbitals due to twisting, and high-curvature at the edges, play little role in the gapping of twisted $(2N,0)$ GNRs with closed armchair edges, i.e., collapsed $(N,0)$ CNTs.

V. CONCLUSION

In summary, we have performed DFTB objective MD calculations on GNRs with H-terminated open and closed armchair edges. These calculations are complementing our previous studies[18,19] to show that the effective strain concept allows for a unified understanding of the electromechanical properties of non-ideal GNRs. In the mechanical domain, we reveal with eq. (2) that the axial strain associated to the unusual inverse Poynting effect for these nanostructures is related to the ε^{eff} stored in the one-atom thick layer. A supportive energetic analysis on twisted GNRs with open edges shows that the mechanical response is dominated by ε^{eff}, although the twist induced misalignment between π orbitals is non-negligible. In the electrical domain, both GNR types exhibit linear YH band gap modulations in the ε^{eff} space, making it possible to establish relations with the known response of ideal cylindrical CNTs and flat GNRs in tension. We note that the effect uncovered here was not visible in the previous study of twisted GNRs in Möbius-like topologies[9]. Since the ring GNRs were allowed to fully relax, the average in-plain strain, similar to ε^{eff}, was vanishingly small and didn't contribute to the reported strain energies and band gap openings.

We thank NSF CAREER Grant CMMI-0747684 and AFOSR Grant FA9550-09-1-0339. Computational resources from University of Minnesota Supercomputing Institute were used.

* Corresponding author. E-mail: td@me.umn.edu.

2 A. Chuvilin, E. Bichoutskaia, M. C. Gimenez-Lopez, T. W. Chamberlain, G. A. Rance, N. Kuganathan, J. Biskupek, U. Kaiser, and A. N. Khlobystov, *Nature Matt.* **10**, 687692 (2011).

3 W. J. Yu, S. H. Chae, D. Perello, S. Y. Lee, G. H. Han, M. Yun, and Y. H. Lee, *ACS Nano* **4**, 5480 (2010).

4 P. A. Williams, S. J. Papadakis, A. M. Patel, M. R. Falvo, S. Washburn, and R. Superfine, *Phys. Rev. Lett.* **89**, 255502 (2002).

5 J.C. Meyer, M. Paillet, and S. Roth, *Science* **309**, 1539 (2005).

6 T. Cohen-Karni, L. Segev, O. Srur-Lavi, S. R. Cohen, and E. Joselevich, *Nat. Nanotechnol.* **1**, 36 (2006).

7 K. S. Nagapriya, S. Berber, T. Cohen-Karni, L. Segev, O. Srur-Lavi, D. Tománek, and E. Joselevich, *Phys. Rev. B* **78**, 165417 (2008).

8 L. Yang and J. Han, *Phys. Rev. Lett.* **85**, 154 (2000).

9 E.W.S. Caetano, V.N. Freire, S.G. dos Santos, D.S. Galvão, and F. Sato, *J. Chem. Phys.* **128**, 164719 (2008).

10 T. Dumitrică and R.D. James, *J. Mech. Phys. Solids* **55**, 2206 (2007).

11 D.-B. Zhang, M. Hua, and T. Dumitrică, *J. Chem. Phys.* **128**, 084104 (2008).

12 D. Porezag, Th. Frauenheim, Th. Köhler, G. Seifert, and R. Kaschner, *Phys. Rev. B* **51**, 12947 (1995).

13 A. Carlson and T. Dumitrică, *Nanotechnol.* **18**, 065706 (2007).

14 R. Rurali and E. Hernandez, *Comp. Mat. Sci.* **28**, 85 (2003).

15 D.-B. Zhang, R.D. James, and T. Dumitrică, *Phys. Rev. B* **80**, 115418 (2009). D.-B. Zhang and T. Dumitrică, *Phys. Rev. B* **82**, 193401 (2010).

16 R.D. James, *J. Mech. Phys. Solids* **54**, 2354 (2006).

17 J.H. Poynting, *Proc. R. Soc. Lond. A* **82**, 546 (1909).

18 D.-B. Zhang and T. Dumitrică, *Small* **7**, 1023 (2011).

19 D.-B. Zhang and T. Dumitrică, *ACS Nano* **4**, 6966 (2010).

20 D.-B. Zhang, E. Akatyeva, and T. Dumitrică, *Phys. Rev. Lett.* **106**, 255503 (2011).

21 S. Jun, X. Li, F. Meng, and C.V. Ciobanu, *Phys. Rev. B* **83**, 153407 (2011).

22 L. Sun, Q. Li, H. Ren, H. Su, Q. W. Shi, and J. Yang, *J. Chem. Phys.* **129**, 074704 (2008).

23 Y. Lu and J. Guo, *Nano Res.* **3**, 189 (2010).

24 P.E. Lammert, P. Zhang, and V.H. Crespi, *Phys. Rev. Lett.* **84**, 2453 (2000).

25 J.A. Elliott, J.K.W. Sandler, A.H. Windle, R. J. Young, and M.S.P. Shaffer, *Phys. Rev. Lett.* **92**, 095501 (2004).

FIG. 1: (a) Axial strain ε^{Py} versus twist rate square γ^2 (left) and shear strain square ε^2 (right) for cylindrical (12,0), (24,0), (36,0), and (48,0) CNTs. (b) Fundamental band gap modulations cylindrical (48,0) CNTs under twisting with DFTB objective MD calculations with fixed and relaxed |**T**|.

FIG. 2: (a) Side and axial view of 28 deg/nm twisted GNR with $N = 12$ dimer lines and two armchair open edges saturated with H. The axis is along the dash-dot line. The repeating objective domain is shaded. Along the directions delineated by the dimer lines, distances between carbon atoms in the neighboring cells varies from 4.48 Å (outmost n=1 line) to 4.26 Å (central $n = 6$ line). The insert shows that the π orbitals located on selected carbon atoms are misaligned. (b) Computed effective tensile strain (solid curve) versus γ under the length fixed constraint. The axial strain $-\varepsilon^{Py}$ (black dash curve) describes the inverse Poynting effect.

FIG. 3: (a) Side view of 8.1 deg/nm twisted 96 GNR with closed armchair edges [a (48,0) collapsed CNT]. The axis is along the dash-dot line. (b) Distribution of the local tensile strain around the circumference computed under fixed (filled squares) and relaxed (empty squares) |**T**| conditions. (c) Computed effective tensile strain (solid line) versus γ under the length fixed |**T**| constraint. The $-\varepsilon^{Py}$ (black dash line) describes the inverse Poynting effect.

FIG. 4: Derivative of the total energy E_{tot} to (a) twist rate γ and (b) to the effective tensile strain ε^{eff}, for 12 GNR with H-saturated armchair edges. The solid line in (b) is $\varepsilon^{eff} C/(1-\nu^2)$. (c) The total energy versus γ. E_{eff} and E_{π} energy components refer to eq. (7).

FIG. 5: Fundamental band gap variations of (a) 12 GNR with H-terminated armchair edges and (b) 96 GNR with closed edges [a collapsed (48,0) CNT] versus twist rate (left) and effective tensile strain (right). In (b) The band gap variation in cylindrical (48,0) CNT in tension predicted with YH model (solid gray curve) is shown for comparison. Calculations were performed at fixed |**T**|.

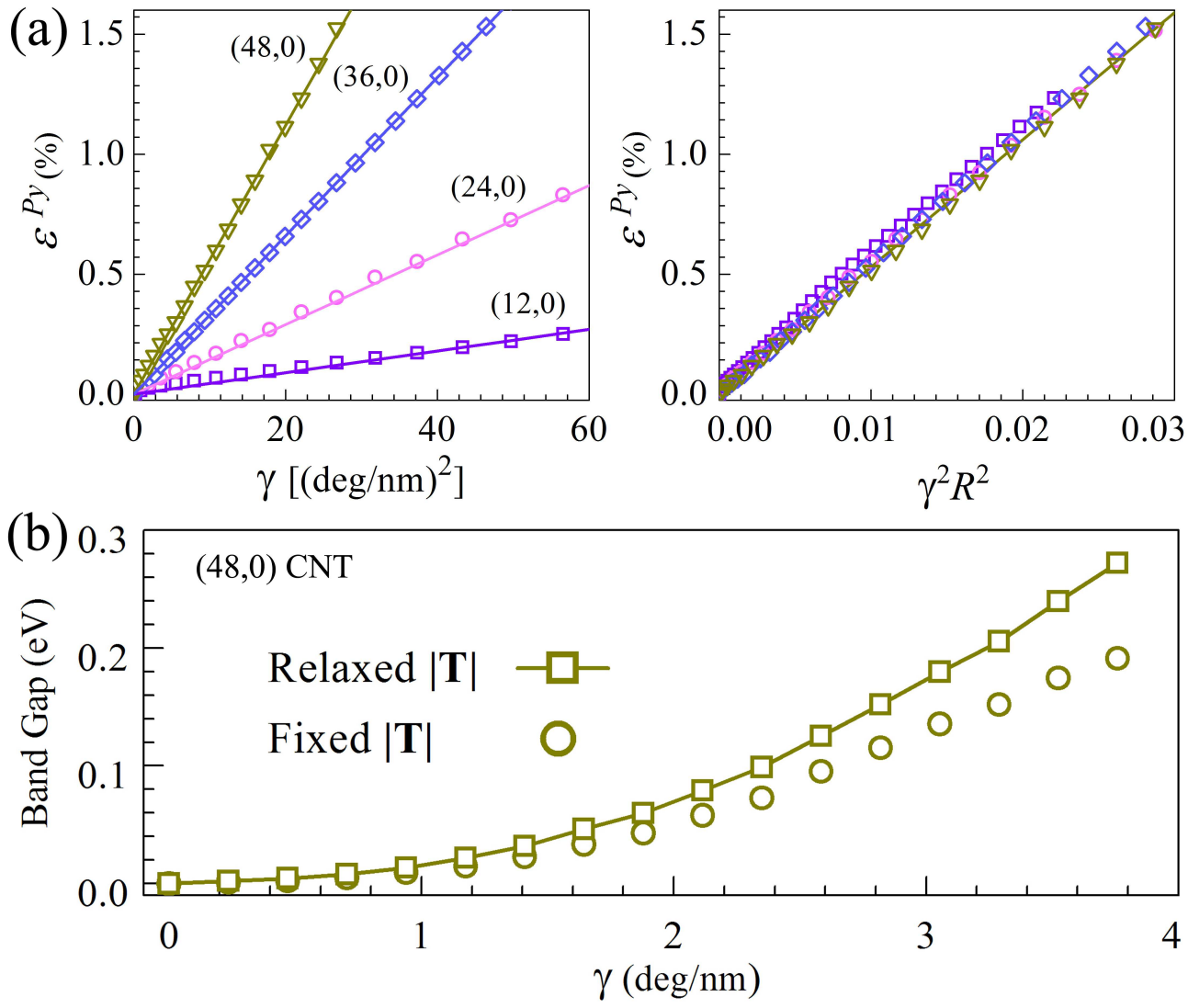

Figure 1 BKJ1150 29Dec2011

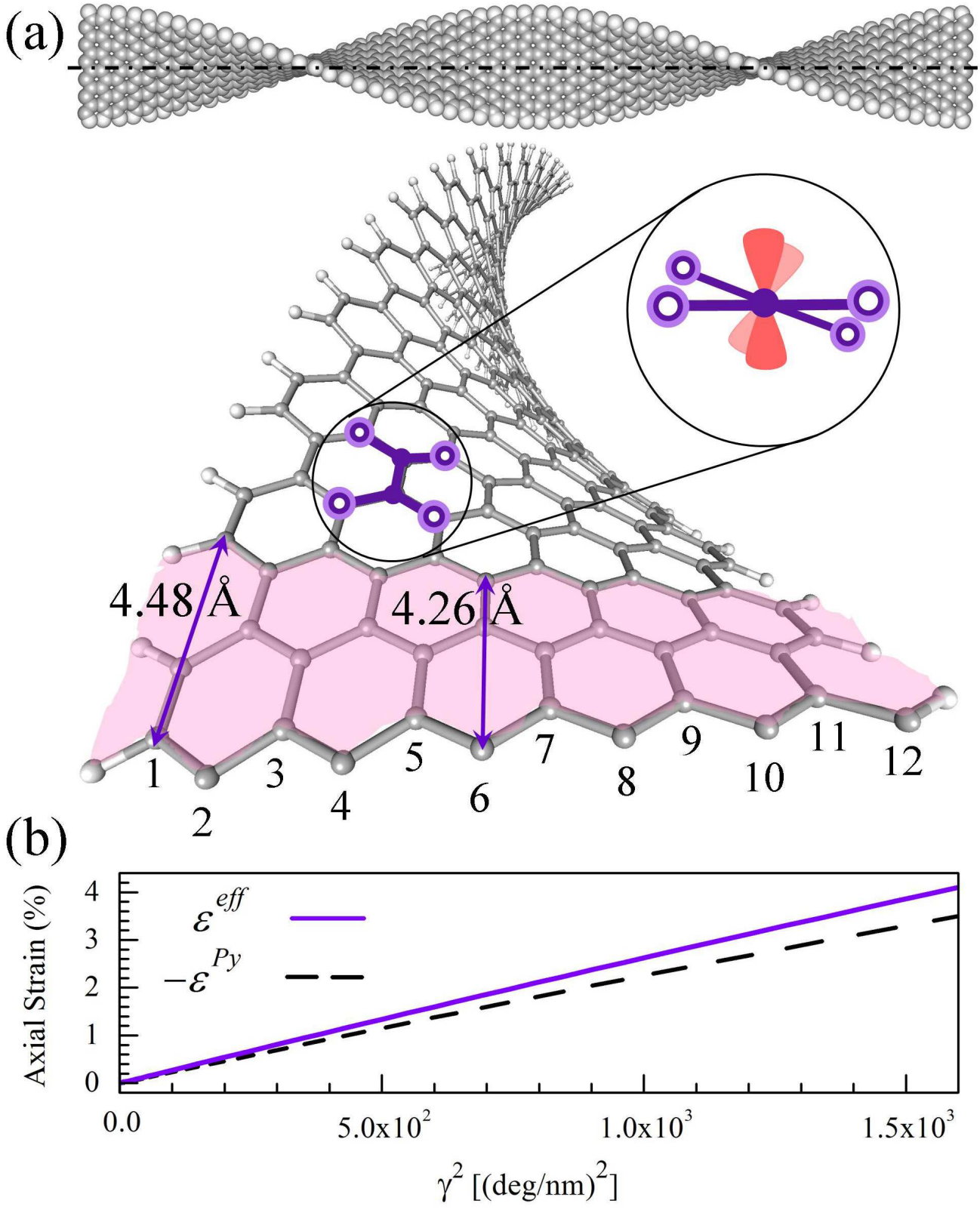

Figure 2 BKJ1150 29Dec2011

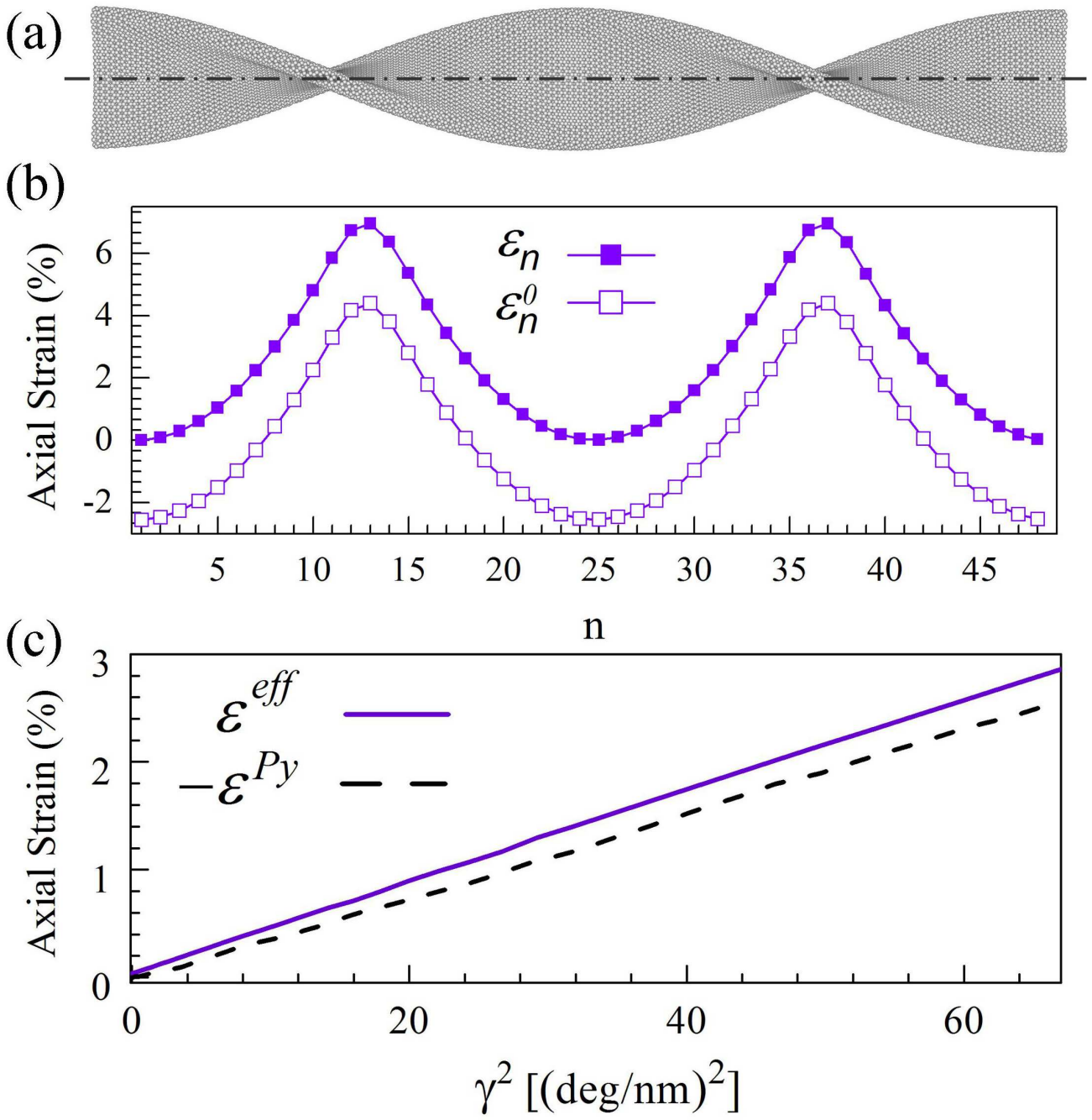

Figure 3 BKJ1150 29Dec2011

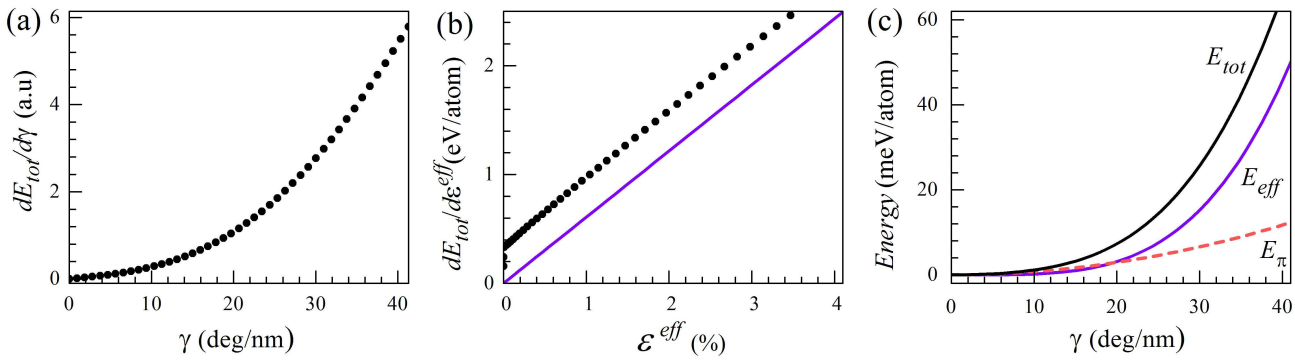

Figure 4 BKJ1150 29Dec2011

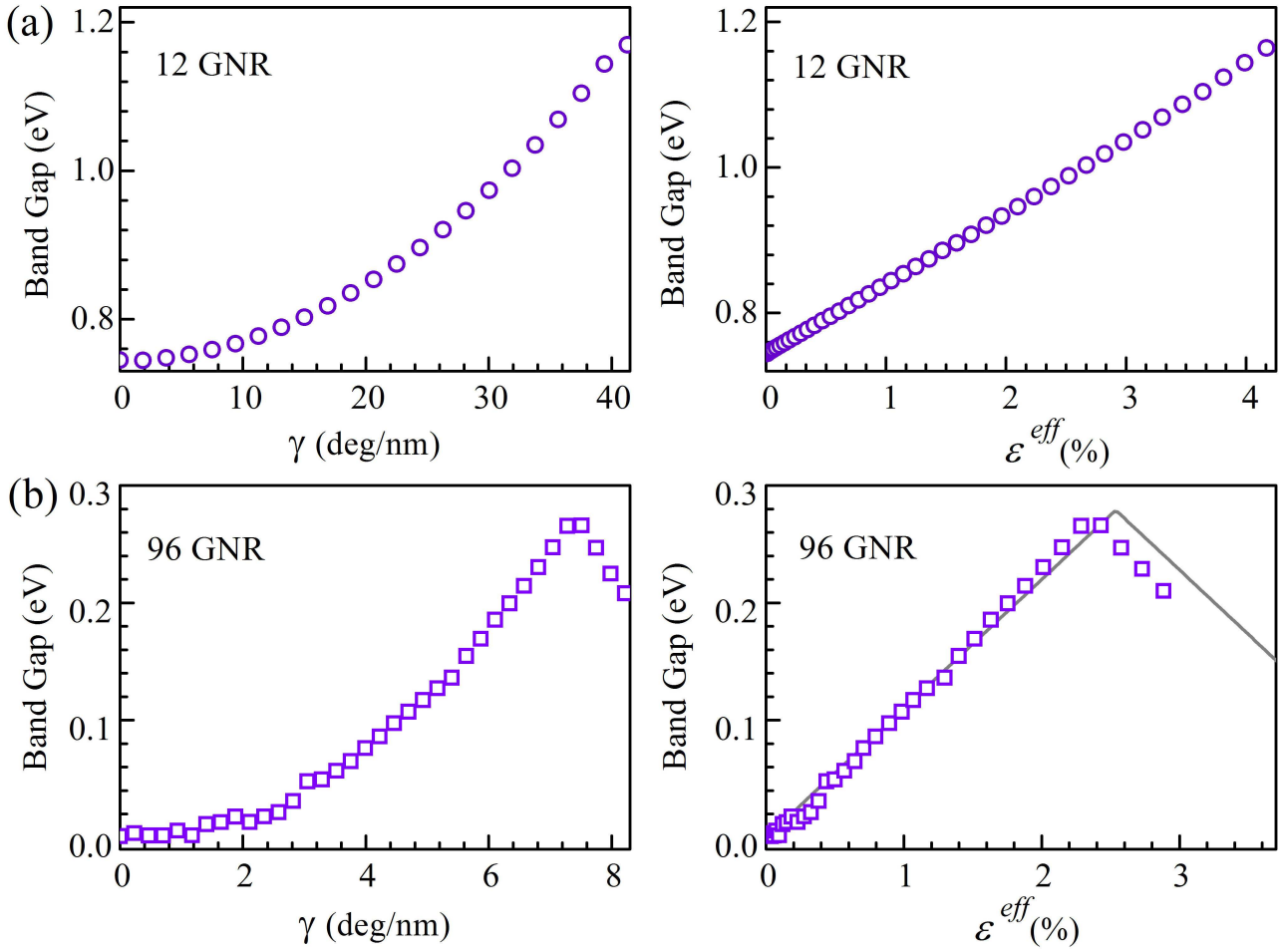

Figure 5 BKJ1150 29Dec2011